Weierstraß-Institut
für Angewandte Analysis und Stochastik

im Forschungsverbund Berlin e.V.

Preprint ISSN 0946 – 8633

Accurate Localization of Brain Activity in Presurgical fMRI by Structure Adaptive Smoothing

Karsten Tabelow[1] [5], Jörg Polzehl [1], Aziz M. Uluğ [2], Jonathan P. Dyke [3], Richard Watts [4], Linda A. Heier [2], Henning U. Voss [3]

submitted: 6th April 2006

[1] Weierstrass Institute
for Applied Analysis and Stochastics,
Mohrenstr. 39, 10117
Berlin, Germany
E-Mail: tabelow@wias-berlin.de

[2] Dept. of Radiology,
Weill Medical College of Cornell University,
New York, NY, United States

[3] Citigroup Biomedical Imaging Center,
Weill Medical College of Cornell University,
New York, NY, United States

[4] Dept. of Physics and Astronomy,
University of Canterbury,
Canterbury, New Zealand

No. 1119

Berlin 2006

[5]Supported by the DFG Research Center MATHEON "Mathematics for key technologies" in Berlin

2000 *Mathematics Subject Classification.* 62P10, 92C55, 62G05, 62G10 .

Key words and phrases. functional MRI, spatially adaptive smoothing, signal detection, presurgical planning.

Edited by
Weierstraß-Institut für Angewandte Analysis und Stochastik (WIAS)
Mohrenstraße 39
10117 Berlin
Germany

Fax: + 49 30 2044975
E-Mail: preprint@wias-berlin.de
World Wide Web: http://www.wias-berlin.de/

Abstract

An important problem of the analysis of fMRI experiments is to achieve some noise reduction of the data without blurring the shape of the activation areas. As a novel solution to this problem, recently the propagation-separation (PS) approach has been proposed. PS is a structure adaptive smoothing method that adapts to different shapes of activation areas by generating a spatial structure corresponding to similarities and differences between time series in adjacent locations. In this paper we demonstrate how this method results in a more accurate localization of brain activity. First, it is shown in numerical simulations that PS is superior over Gaussian smoothing with respect to the accurate description of the shape of activation clusters and results in less false detections. Second, in a study of 37 presurgical planning cases we found that PS and Gaussian smoothing often yield different results, and we present examples showing aspects of the superiority of PS as applied to presurgical planning.

1 Introduction

Functional magnetic resonance imaging (fMRI) has become a versatile non-invasive tool for studying the functionality of the brain and for localizing cognitive functions. Nowadays, fMRI is not only used in the neurosciences but also in applications such as presurgical planning. For example, in neuro-oncologic brain surgery Vlieger et al. (2004); Haberg et al. (2004); Bogomolny et al. (2004), the goal is to maximize tumor resection or to perform epilepsy surgery while preserving important brain functions. Presurgical fMRI can be used to localize motor, sensory, and language-control areas Henson et al. (2005), and has been used to study cerebral reorganization in tumor patients Baciu et al. (2003).

In general, activation in the brain is indirectly measured by utilizing the blood oxygenation level dependent (BOLD) effect as a natural contrast sensitive to neural activity Ogawa et al. (1990, 1992). The data, time series of three-dimensional volumes, are characterized by a low signal-to-noise ratio, in particular if a high resolution is desired. Due to the low signal-to-noise ratio, fMRI signal detection requires using spatial information, or smoothing. However, the commonly used smoothing by a Gaussian filter improves signal detection at the cost of blurring, the loss of information on the spatial extent and shape of the activation area. As an alternative, here we apply a spatially adaptive smoothing

procedure, the propagation-separation (PS) approach Polzehl and Spokoiny (2000, 2005), to presurgical fMRI data of 37 epilepsy/tumor/vascular malformation patients. The procedure achieves a similar variance reduction as Gaussian smoothing but is able to adapt to different shapes of activation areas by generating a spatial structure corresponding to similarities and differences between time series in adjacent locations. Using this approach in the analysis of fMRI data was first suggested in Polzehl and Spokoiny (2001) and generalized in Tabelow et al. (2006b), followed by a preliminary application involving presurgical fMRI data Tabelow et al. (2006a).

In presurgical planning of tumor resection it is of importance to have a high test power to avoid false positive (in particular in the lesion) and a high specificity to prevent false negative (in particular outside the lesion) activations. Due to the clinical circumstances, usually simple to understand and strong activation paradigms are used, such as finger tapping, word rhyming, or picture naming. In patients, motion, fatigue, and degree of cooperation may play a more significant role than in volunteers in well-controlled neuroscience studies, and results must be interpreted with greater care. These circumstances sometimes even render the detection of activated areas in simple and strong activation paradigms difficult. This is even more serious as the sensitivity of fMRI measurement directly affects the detectability and reproducibility of the activation area, which will affect clinical decisions.

In numerical simulations, we show that PS is superior over Gaussian smoothing with respect to the accurate description of the shape of activation clusters and less false detections. The positive numerical results were reproduced in the application to presurgical fMRI data, where we found that PS and Gaussian smoothing give significantly different results for almost all datasets. We could identify examples which showed different aspects of the enhanced accuracy of PS in presurgical planning.

The paper is organized as follows. Section 2 shortly explains the acquisition of fMRI used in the application. Section 3 summarizes the statistical evaluation of fMRI data, the application of PS and its theoretical background. Section 4 discusses properties of the approach using an artificial data set and provides results obtained for presurgical fMRI data.

2 Data Acquisition

We investigated pre-surgical functional MRI scans of 26 tumor patients, 5 patients with vascular malformations, and 6 epilepsy patients. Images were acquired on a GE 3T scanner

using a 2D gradient echo EPI sequence with TE/TR = 40/2000 or 40/3000 ms. 24 to 34 axial slices of 4 or 5 mm thickness and a matrix size of 64 x 64 were acquired. Tasks were performed in three blocks during 3.7 min of scanning time. The block length was 30s on and 30s off, repeated three times after an initial off block of 42s. The first 4 scans were discarded to accomplish equilibrium of the spin dynamics, yielding 107 or 70 repetitions in total. The tasks were: motor (bilateral or right hand only tapping of thumb against all fingers of same hand), a language task (forming words beginning with given letter), another language task (rhyming with a given word), and a visual task (naming of pictures). Motor tasks where performed in all patients, language and visual task in most but not all patients.

3 Statistical evaluation

In BOLD-fMRI the expected BOLD response $x(t)$ can be modeled by a convolution of the task indicator function $s(t)$ with the hemodynamic response function $h(t)$. After reconstruction of the raw data, motion correction, and image registration, the linear model

$$Y_{it} = X\beta_i + \epsilon_{it} \tag{1}$$

is used to describe the time series $Y = (Y_t)_{t=1,\ldots,T}$ in voxel i. The design matrix X specifies the *expected BOLD response* for the experimental stimulus, as well as additional effects to model mean level and drift. The noise ϵ_{it} is correlated in time, due to the short acquisition times. Thus a prewhitening based on an AR(1) model is performed. From the linear model we obtain estimates of effects $\widetilde{\gamma}_i = c^T\widetilde{\beta}_i$ and the corresponding standard deviations $\widetilde{s}_i = (c^T \operatorname{Var}\widetilde{\beta}_i c)^{1/2}$ by least squares at each voxel i. The constant c is a vector of contrasts to define the effects of interest **?**.

The results from the voxelwise analysis can be arranged as three dimensional arrays $\widetilde{\Gamma}$, $\widetilde{S}$. The statistical parametric map (SPM) $\widetilde{\Theta}$ formed from the voxelwise quotients $\widetilde{\theta}_i = \widetilde{\gamma}_i/\widetilde{s}_i$ can be viewed as a random t-field Worsley (1994), carrying a correlation structure induced by the spatial correlation in the fMRI data. However, in situations where activations have a spatial extent, spatial smoothing of the array $\widetilde{\Gamma}$ has the potential to improve both overall sensitivity and specificity of signal detection.

In Tabelow et al. (2006b) the use of a spatial adaptive smoothing procedure derived from the PS approach Polzehl and Spokoiny (2005) has been proposed in this context. The approach focuses, for each voxel i, on simultaneously identifying a region where the unknown parameter γ is approximately constant and to obtain an optimal estimate $\widehat{\gamma}_i$ employing this structural information. This is achieved by an iterative procedure. Local smoothing

is restricted to local vicinities of each voxel, that are characterized by a weighting scheme. Smoothing and characterization of local vicinities are alternated. Weights for a pair of voxels i and j are constructed as a product of kernel weights $K_{\mathrm{loc}}(\delta(i,j)/h)$, depending on the distance $\delta(i,j)$ between the two voxels and a bandwidth h, and a factor reflecting the difference of the estimates $\widehat{\gamma}_i$ and $\widehat{\gamma}_j$ obtained within the last iteration. The bandwidth h is increased with iterations up to a maximal bandwidth h_{max}.

"Propagation-separation" denotes the two main properties of this algorithm. In case of a completely homogeneous array $\widetilde{\Gamma}$, the algorithm delivers essentially the same result as a nonadaptive kernel smoother employing the bandwidth h_{max}. In this case the procedure selects the best of a sequence of almost nonadaptive estimates, that is, it propagates to the one with maximum bandwidth. Separation means that as soon as within one iteration step significant differences of $\widehat{\gamma}_i$ and $\widehat{\gamma}_j$ are observed the corresponding weight is decreased to zero and the information from voxel j is no longer used to estimate γ_i. Voxels i and j belong to different regions of homogeneity and are therefore separated. As a consequence smoothing is restricted to regions with approximately constant values of γ, bias at the edge of such regions is avoided and the spatial structure of activated regions is preserved. Numerical complexity, as well as smoothness within homogeneous regions is controlled by the maximal bandwidth $h_{\max}$.

Adaptive spatial smoothing results in arrays $\widehat{\Gamma} = (\widehat{\gamma}_i)$ and $\widehat{S} = (\widehat{s}_i)$. Signal detection can now be based on the random field $\widehat{\Theta} = (\widehat{\gamma}_i/\widehat{s}_i)$. If no activation is present in any voxel, that is, the hypothesis H: $\gamma_i = 0$ holds for all i, the properties of $\widehat{\Gamma}$ and $\widehat{S} = (\widehat{s}_i)$ approximately coincide with properties of the corresponding arrays obtained by nonadaptive smoothing with bandwidth h_{max}. As an effect of spatial smoothing the distribution of $\widehat{s}_i$ has, compared to the distribution of $\widetilde{s}_i$, a much larger number of degrees of freedom. The t-field $\widehat{\Theta}$ can therefore be well approximated by a Gaussian random field. Approximate p-values can be associated with a signal in voxel i employing results on the exceedance probability for maxima of stationary Gaussian random fields Worsley et al. (1996); Tabelow et al. (2006b).

For a formal description of this algorithm, a discussion of its properties and theoretical results we refer to Tabelow et al. (2006b).

Data was pre-processed using AFNI Cox (1996) and analyzed by a package Polzehl and Tabelow (2006) for the R-statistical environment R Development Core Team (2005).

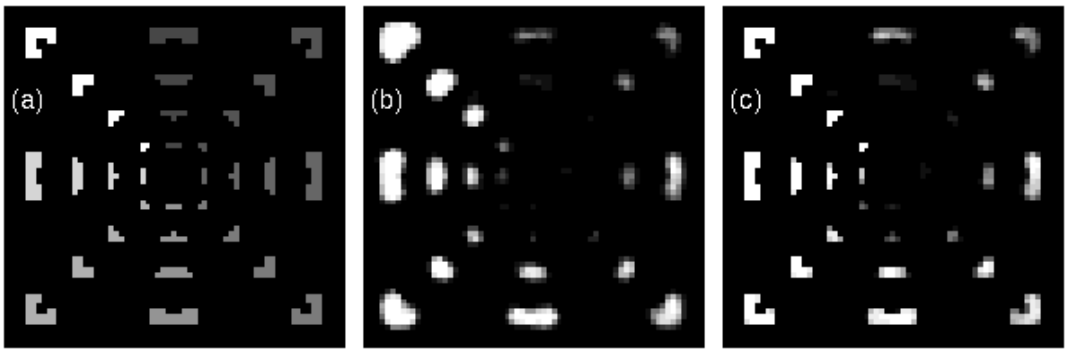

Figure 1: A numerical phantom for studying the performance of PS vs. Gaussian smoothing. (a) Eight different signal-to-noise ratios, increasing clockwise, are coded by gray values. The spatial extent of activations varies in the radial direction. (b) Smoothing with conventional Gaussian filter. (c) Smoothing with PS. In both (b) and (c), the bandwidth is 3 voxels which corresponds to FWHM = 10 mm for typical voxel size. In (b) and (c) the proportion of voxels that are detected in a given position, over 15 slices containing activations, is rendered by gray values. Black corresponds to the absence of a signal.

4 Results

4.1 Artificial data

The application of PS and Gaussian smoothing to a numerical phantom is demonstrated in Fig. 1. The phantom consists of a three dimensional dataset, in which a slice containing activation is replicated three times in the z-direction, followed by two slices with no activation, etc. The position of activated regions within the slices and amplitudes of the signal are illustrated in Fig. 1a. The form and size of activation areas change radially, whereas the signal-to-noise ratio increases clockwise. At each of these voxels a time series was created with 107 scans, stimulus onset times at the 18th, 48th, and 78th scan with a stimulus duration of 15 scans and 2 s between two scans. This directly corresponds to the paradigm most frequently used in the presurgical data. Autoregressive temporal noise has been added, while spatial correlation was introduced to model effects of data acquisition and preprocessing. Fig. 1b shows the result of the signal detection after smoothing the SPM with a Gaussian filter using a FWHM bandwidth of 3 voxel sizes. The gray level corresponds to the relative frequency of signal detection obtained by averaging over all slices that contain activations. Whereas signals from small areas with very low signal-to-noise ratio are practically not detected, the shapes of the detected activation areas are not well reproduced. In particular, concave structures are oversmoothed.

In contrast to this result, the signal detection after smoothing with PS achieves a sim-

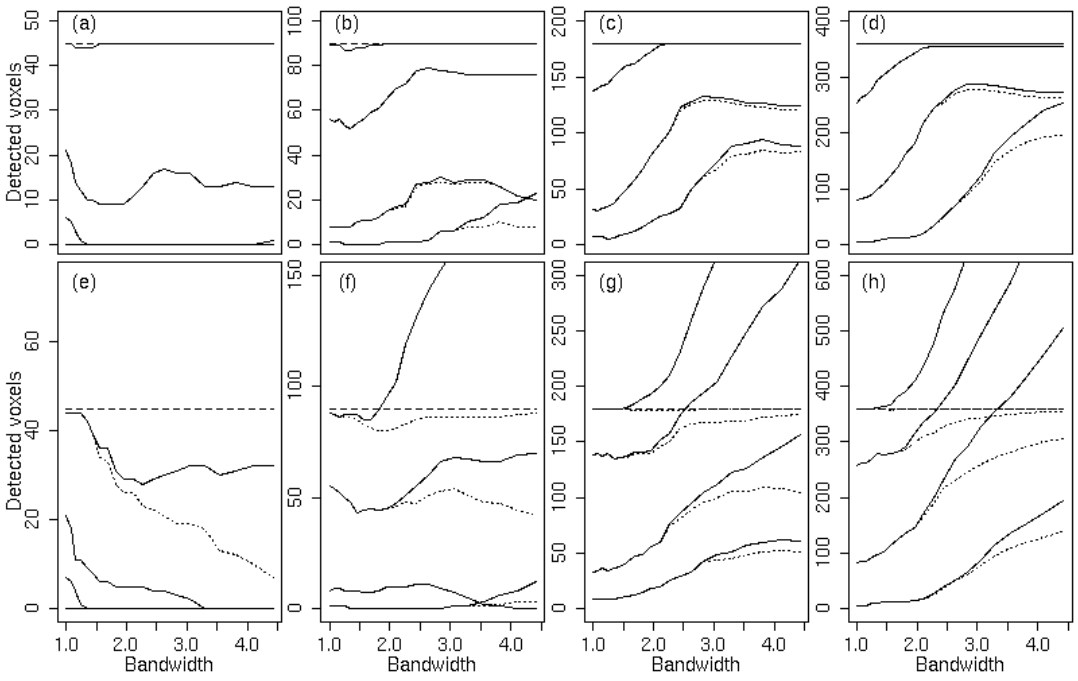

Figure 2: Number of detected voxels for PS (a) to (d), and Gaussian filter (e) to (h) as described for Fig. 1 as a function of bandwidth h_{max}. Activation area size grows from left to right corresponding to the radial direction in Fig. 1. The four curves correspond to increasing signal-to-noise ratios present in the areas on the four diagonal lines in Fig. 1a. The SNR increases for curves from bottom to top in each plot. The correct number of activations is shown as a dashed line. The dotted lines show the number of correctly detected active voxels.

ilar sensitivity but preserves the shape and size of activation areas (Fig. 1c). Since the procedure naturally adapts to different sizes, smaller and larger areas can be detected simultaneously using the same maximum bandwidth h_{max}.

Figure 2 shows the number of detected voxels as a function of the applied maximum bandwidth for different area sizes and different signal-to-noise ratios. The total number of detections in and within a vicinity of activated regions are given by solid lines whereas the number of correctly detected voxels is presented as a dotted line. The upper row shows the results using PS, while for the lower row a Gaussian filter was applied. The size of the activated area increases from left to right, corresponding to the radial direction in the phantom (Fig. 1a). The four curves correspond to increasing signal-to-noise ratios present in the areas on the four diagonal lines in Fig. 1a). The simulation results illustrate that for strong signals both methods achieve a similar sensitivity. PS clearly avoids most of the false positives generated by the Gaussian filter in case of larger bandwidths. Additionally, it does not show the dependence between optimal bandwidth, SNR and size of the activation area that is typically observed in case of the Gaussian filter. We conclude that the

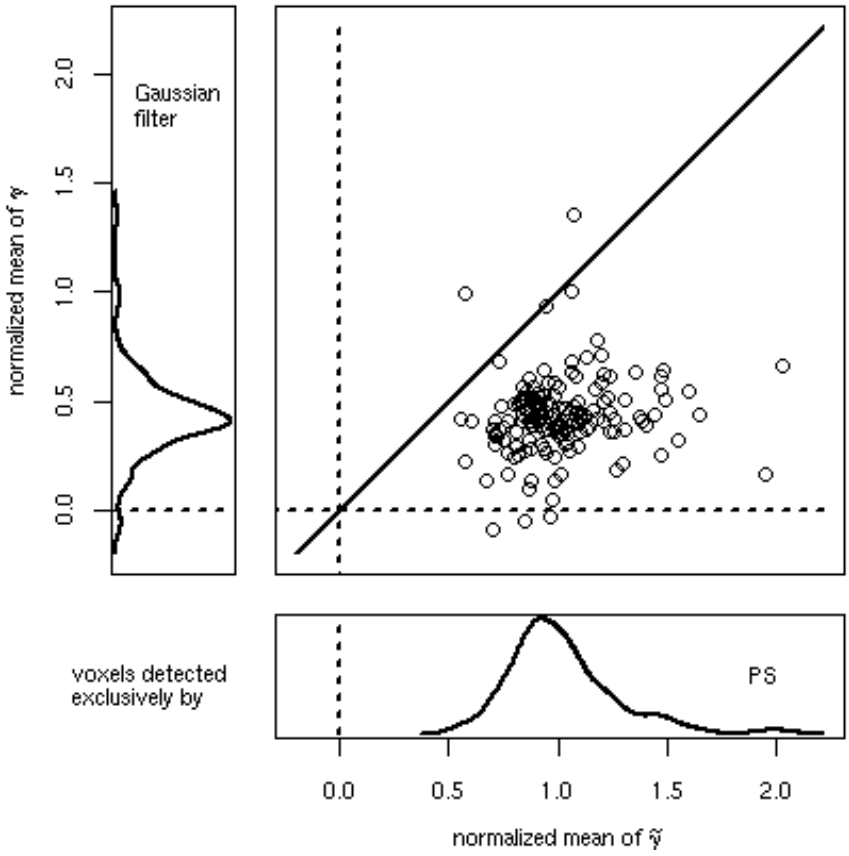

Figure 3: Ratios of the mean of voxelwise estimates $\widetilde{\gamma}$ over voxels detected exclusively by Gaussian filter (vertical coordinate) and PS (horizontal coordinate) and the mean of voxelwise estimates $\widetilde{\gamma}$ over voxels detected by both methods. Each point in the scatter plot corresponds to one of the 155 datasets. Marginal densities are provided additionally. Results are generated using $p = 0.001$ and $h = 10$ mm in all experiments.

maximum bandwidth can be chosen as FWHM of 2-3 times the voxel size, as usual.

4.2 Presurgical fMRI data

We analyzed experimental data from 37 presurgical cases with a total number of 155 datasets. Figure 3 summarizes the different behavior of smoothing by PS and Gaussian filtering over all datasets. Each point in the scatter plot corresponds to one dataset. The coordinates of each point are determined by the ratio between the mean of the unsmoothed estimates $\widetilde{\gamma}$ over voxels exclusively detected by one of the methods and the mean of the unsmoothed estimates $\widetilde{\gamma}$ that are detected by both methods. The horizontal axis corresponds to using PS whereas the vertical axis gives the ratio for the Gaussian filter. Additionally, marginal densities for the ratios are shown in both cases. As a result, the mean of $\widetilde{\gamma}$ over voxels exclusively detected by use of PS varies around the mean of $\widetilde{\gamma}$ over voxels detected

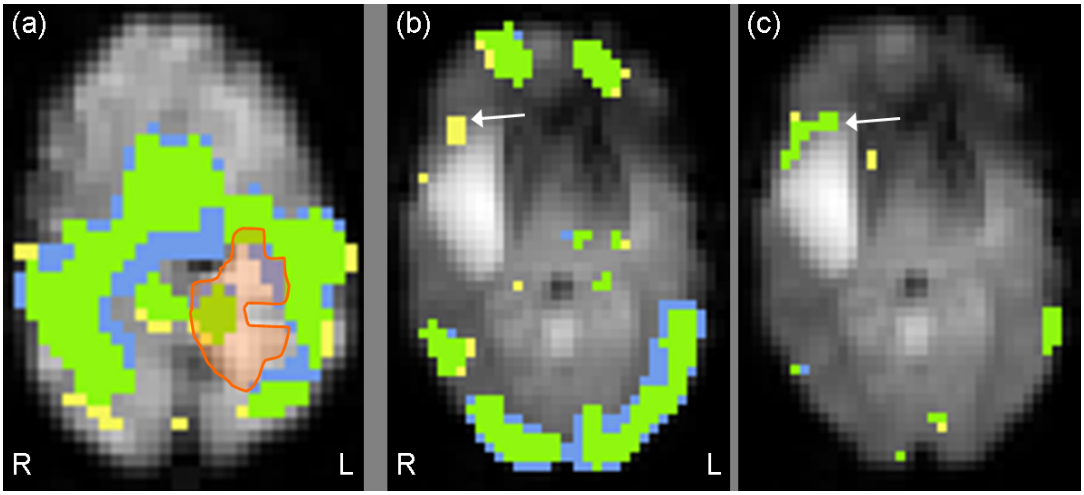

Figure 4: Examples of activations seen only with Gaussian smoothing (blue), only with PS (yellow), and with both methods (green). (a) In the bilateral finger tapping task, PS (yellow) and Gaussian smoothing alone (blue) yielded different results in the vicinity of the tumor which is delineated by the red area. (b, c) In the picture naming task, PS detected activation next to a tumor ((b), arrow) which was not seen with Gaussian smoothing. The potential neuronal activity of this region is known from a motor task (bilateral finger tapping), in which both methods detected this area ((c), arrow); thus, Gaussian smoothing probably yielded false negative activations. In all plots $p = 0.001$, $h = 10$ mm.

by both methods (that is, the data points cluster around 1.0), whereas voxels detected exclusively using a Gaussian filter correspond to considerably smaller voxelwise estimates. Although we do not have a gold standard, it is reasonable to interpret this difference as a more likely presence of false positives in the Gaussian filter case.

Examples are illustrated in Figs. 4 to 6. Figure 4 demonstrates the effects of using PS (yellow plus green area) or a Gaussian filter (blue plus green area) in the vicinity of tumors. The green areas constitute the intersection of the two methods. In this example, Gaussian smoothing and PS yield rather different results in and around a tumor. In Fig. 4a, Gaussian smoothing seems to oversmooth into areas occupied by tumor (delineated by a red line), whereas PS renders the tumor boundary better. However, there are cancerous regions into which both methods reach (green area). Another frequently observed result is that, although the sensitivity of PS is not generally larger than Gaussian smoothing, there are regions next to the tumor that are detected with PS only (Fig. 4b, visual task). The potential neuronal activity of this region is known from a motor task (bilateral finger tapping), in which both methods detected this area (Fig. 4c). If this area was indeed active during the visual task, Gaussian smoothing yielded false negative activations.

Figure 5 demonstrates the enhanced capability of PS to resolve complex anatomic struc-

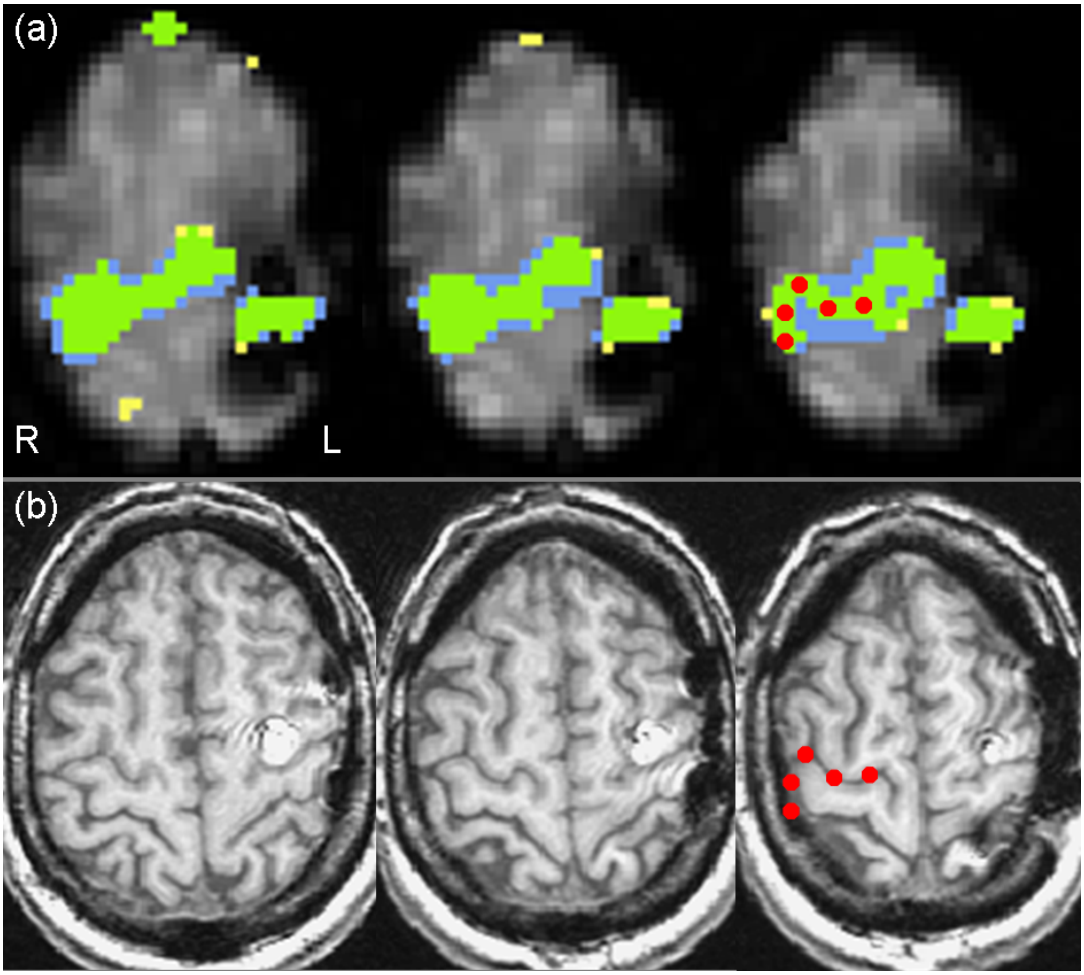

Figure 5: Three consecutive EPI slices with functional activations (a) and corresponding anatomical images (b) of the brain of an epilepsy patient during a bilateral finger tapping task. It is evident that the activations in the cortical areas of the pre- and postcentral gyrus, next to the central sulcus, are better delineated in PS (yellow and green) than in Gaussian smoothing (blue and green), in particular in the third slice, nearest to the brain surface (red dots). (In all images, $p = 0.001$, $h = 10$ mm. Again, activations seen only with Gaussian smoothing are depicted in blue, seen only with PS in yellow, and seen in both methods in green. The signal dropout is caused by susceptibility artifacts from a prior craniotomy.

tures. In a bilateral finger tapping task, the meandering cortical gray matter areas of the pre- and postcentral gyrus next to the central fissure (motor and somatosensory strip, respectively) are better delineated in PS (yellow and green) than in Gaussian smoothing (blue and green).

Finally, Fig. 6 shows functional activations of a patient with arteriovenous malformations, which often yield a relatively large BOLD effect, during a bilateral finger tapping task. Generally, the detections obtained by Gaussian smoothing reach far into white matter

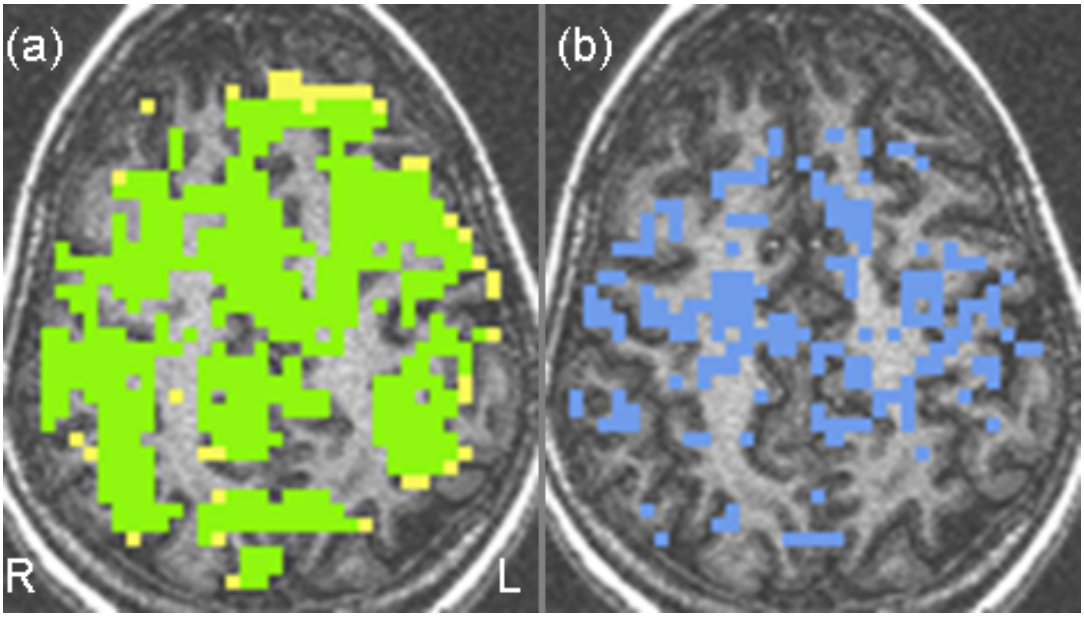

Figure 6: Functional activations obtained with both PS and Gaussian smoothing (a) and with Gaussian smoothing only (b), of the brain of a patient with an arteriovenous malformation during a bilateral finger tapping task. The activation as detected with PS (yellow and green in (a)) delineates the gray matter regions of the brain much better than the activations as detected with Gaussian smoothing, which covers also white matter areas. (In both plots $p = 0.001$, $h = 10$ mm. Again, activations seen only with Gaussian smoothing are depicted in blue, seen only with PS in yellow, and seen in both methods in green.)

areas, whereas the detections obtained with PS appear to be much more confined to gray matter areas.

5 Conclusion and Discussion

We have shown on numerical examples and a study involving 37 patients that the analysis of presurgical functional MRI data by structure adaptive weight smoothing (PS) yields more accurate results as compared to the conventional approach of Gaussian smoothing. As any filtering method, the application of spatially adaptive smoothing increases the signal to noise ratio. In addition, it also preserves the effective spatial resolution of activated areas. The main finding is that the detected activations obtained with PS are more confined to given gray matter cortical structures. Furthermore, frequently the activity next to tumors was detected with a higher reliability.

Whereas due to the matched filter theorem, the bandwidth of a non-adaptive Gaussian filter is best chosen as the size of the usually not precisely known expected activation,

PS naturally adapts to different sizes of activated areas. In the analysis with PS the resulting statistical parametric map depends on the order in which spatial smoothing and voxelwise parameter estimation are performed. To conduct the analysis of the voxelwise time series first, as done here, has two advantages: It leads to a dimension reduction that enables the use of adaptive smoothing techniques and it provides a situation where spatial smoothing increases the degrees of freedom in the resulting random t-field, enabling the use of Gaussian random fields for thresholding Tabelow et al. (2006b).

It is worth investigating if the problem of false negative activations next to tumors in the primary sensorimotor cortex Holodny et al. (1999), which is probably caused by an altered hemodynamic response due to the tumor vascularity Fujiwara et al. (2004), can be alleviated with PS. Future work will also concentrate on the applicability of anisotropic PS procedures to related problems in diffusion tensor imaging Basser et al. (1994); Watts et al. (2003), where estimation of the diffusion tensor could benefit from a structure dependent smoothing of the low-signal-to-noise ratio diffusion weighted images. This may be of importance in particular for the challenge of finding motor and other pathways Holodny et al. (2005) and for diffusion tensor imaging in the spinal cord Voss et al. (2006).

Acknowledgments

This work is supported by the DFG Research Center Matheon. H.U.V. acknowledges financial support from the Cervical Spine Research Society.

References

Baciu, M., Bas, J. F. L., Segebarth, C., and Benabid, A. L. (2003). Presurgical fMRI evaluation of cerebral reorganization and motor deficit in patients with tumors and vascular malformations. *Eur. J. Radiol.*, 46:139–146.

Basser, B. J., Mattiello, J., and Le Bihan, D. (1994). Estimation of the effective self-diffusion tensor from the NMR spin echo. *J. Magn. Res. Series B*, 103:247–254.

Bogomolny, D. L. et al. (2004). Functional MRI in the brain tumor patient. *Top. Magn. Reson. Imaging*, 15:325–335.

Cox, R. W. (1996). Afni: Software for analysis and visualization of functional magnetic resonance neuroimages. *Computers and Biomed. Res.*, 29:162–173.

Fujiwara, N. et al. (2004). Evoked-cerebral blood oxygenation changes in false-negative activations in BOLD contrast functional MRI of patients with brain tumors. *Neuroimage*, 21:1464–1471.

Haberg, A., Kvistad, K., Unsgard, G., and Haraldseth, O. (2004). Preoperative blood oxygen level-dependent functional magnetic resonance imaging in patients with primary brain tumors: clinical application and outcome. *Neurosurgery*, 54:902–915.

Henson, J. W., Gaviani, P., and Gonzalez, R. (2005). MRI in treatment of adult gliomas. *Lancet Oncol.*, 6:167–175.

Holodny, A. I. et al. (1999). Decreased BOLD functional MR activation of the motor and sensory cortices adjacent to a glioblastoma multiforme. implications for image-guided neurosurgery. *Am. J. Neuroradiol.*, 20:609–612.

Holodny, A. I. et al. (2005). Diffusion tensor tractography of the motor white matter tracts in man — current controversies and future directions. *Ann. N.Y. Acad. Sci.*, 1064:88–97.

Ogawa, S., Lee, T., Kay, A., and Tank, D. (1990). Brain magentic resonance imaging with contrast dependent on blood oxygenation. *Proc. Nati. Acad. Sci. USA*, 87:9868–9872.

Ogawa, S., Tank, D., Menon, R., Ellermann, J., Kim, S., Merkle, H., and Ugurbil, K. (1992). Intrinsic signal changes accompanying sensory stimulation: Functional brain mapping with magnetic resonance imaging. *Proc. Nati. Acad. Sci. USA*, 89:5951–5955.

Polzehl, J. and Spokoiny, V. (2000). Adaptive weights smoothing with applications to image restoration. *J. Roy. Statist. Soc. Ser. B*, 62:335–354.

Polzehl, J. and Spokoiny, V. (2001). Functional and dynamic magnetic resonance imaging using vector adaptive weights smoothing. *J. Roy. Statist. Soc. Ser. C*, 50:485–501.

Polzehl, J. and Spokoiny, V. (2005). Propagation-separation approach for local likelihood estimation. *Probab. Theory and Relat. Fields, in print: http://dx.doi.org/10.1007/s00440-005-0464-1.*

Polzehl, J. and Tabelow, K. (2006). *Analysing fMRI experiments with the fmri package in R. A users guide.* Weierstrass Institute for Applied Analysis and Stochastics (WIAS), Berlin, Germany. ISSN 1618-7776.

R Development Core Team (2005). *R: A Language and Environment for Statistical Computing.* R Foundation for Statistical Computing, Vienna, Austria. ISBN 3-900051-07-0.

Tabelow, K., Polzehl, J., Spokoiny, V., Dyke, J. P., Heier, L. A., and Voss, H. U. (2006a). Accurate localization of functional brain activity using structure adaptive smoothing. *Submitted to the Proc. of the 14th Scientific Meeting of ISMRM*.

Tabelow, K., Polzehl, J., Voss, H. U., and Spokoiny, V. (2006b). Analyzing fMRI experiments with structural adaptive smoothing procedures. *preprint*.

Vlieger, E. J., Majoie, C., Leenstra, S., and den Heeten, G. J. (2004). Functional magnetic resonance imaging for neurosurgical planning in neurooncology. *Eur. Radiol.*, 14:1143–1153.

Voss, H., Watts, R., Ulug, A. M., and Ballon, D. (2006). Fiber tracking in the cervical spine and inferior brain regions with reversed gradient diffusion tensor imaging. *MRI, in press*.

Watts, R., Liston, C., Niogi, S., and Ulug, A. M. (2003). Fiber tracking using magnetic resonance diffusion tensor imaging and its applications to human brain development. *Ment. Retard. Dev. Disabil. Res. Rev.*, 9:168–177.

Worsley, K. (1994). Local maxima and the expected Euler characteristic of excursion sets of χ^2, f and t fields. *Advances in Applied Probability*, 26:13–42.

Worsley, K., Marrett, S., Neelin, P., and Evans, A. (1996). Searching scale space for activation in PET images. *Human Brain Mapping*, 4:74–90.